Structural characterization of synthesized Al-doped ZnS nanoparticles deposited on glass substrate

M. H. Eisa [a,b*], A. A. Ahmed [a]
[a] *Department of Physics, College of Science, Sudan University of Science and Technology, Khartoum 11113, Sudan*
[b] *Department of Physics, College of Sciences, Imam Mohammad Ibn Saud Islamic University (IMSIU), Riyadh 11623, Saudi Arabia*

This study aimed to determine the effect of Al-doping on the physical properties of ZnS thin films. The pulsed-laser deposition technique was used to prepare ZnS and Al-doped ZnS (AZS) thin films on soda-lime glass slides. The Al concentration of 0–6% was used. Further, XRD spectroscopy was employed to confirm the structures of the ZnS and AZS films, following which the values of parameters such as crystal plane spacing, crystallite grain size, microstrain, and dislocation density were calculated. Regarding ZnS, the result showed a broad pattern corresponding to the (111) plane of ZnS. There was a variation of 0.313–0.316 nm in the d-spacing, which decreased as the concentration of Al in the ZnS films increased. The crystallite size was found to be 0.80–671.24 nm. Notably, the crystallite size was affected by the Al concentration. The change in the a aluminum content from 0 to 8% make change in thee strain increase from 0.00046 to 0.0031. Also, as the Al-doping increased, the dislocation-density reduced from 1.54 to 0.00000221 mg.cm^{-3}. The values obtained in this work were consistent with published standards.

1. Introduction

Nanoparticles (NPs) have attracted great attention in recent times owing to their unique properties. Zinc sulphide (ZnS) NP is a popular compound with favorable semiconductor properties and possesses a direct and wide bandgap. ZnS is generally obtained in two polymorphic forms: zinc blende (β-ZnS) and wurtzite (α-ZnS) [4]. ZnS NP belongs to Group II–VI of chalcogenide materials [5]. Among its several desirable properties are a wide direct bandgap of 3.65 eV, a high refractive index of 2.35 at 632 nm, a wide wavelength passband, and an exciton binding energy of about 40 meV [6-10]. Compared to the "S' anion, the "Zn" cation is smaller. The "S" atoms exhibit a face-centered cubic (FCC) arrangement. Zinc sulphide's characteristics such as cost-efficiency, non-toxicity, environmentally-friendliness, safe for handling, and stability make it ideal for several applications.

The ZnS NP semiconductor's bandgap energy makes it a suitable material for employment as a host matrix for varoius dopants. Previous research on ZnS films has shown that, when silver (Ag), manganese (Mn), and copper (Cu) are used as dopants, ZnS inhibits blue, orange, and green colors, respectively [7, 11, 12]. Recent studies on ZnS have emphasized the usefulness of trivalent metal cations as dopants, including Group III elements such as boron (B) [13], aluminum (Al) [4, 14], indium (In) [15], gallium (Ga) [16], and manganese (Mn) [17]. Overall, the exceptional features of Al-doped ZnS (AZS) make it useful for various applications [4, 14, 18].

Therefore, the influence of aluminum on the characteristics of ZnS NPs should be further investigated. Notably, only a few studies have been conducted on AZS films on glass substrates. In this study, a soda-lime glass slide was selected as the substrate. The undoped ZnS and Al-doped Several methods have been successfully employed for deposition of ZnS thin films such as,

---

the sol-gel method [19], sputtering method [20], spray pyrolysis method [21], thermal evaporation method [22], chemical-bath deposition (CBD) method [23], and pulsed laser deposition (PLD) method [24, 25. Among these, the PLD method is the most efficient method for producing films of complex materials [26]. The PLD is a powerful method for the stoichiometric deposition of materials with multiple components. In this work, ZnS and AZS samples were prepared on the glass substrates using the PLD method. The prepared samples were characterized using XRD method.

2. Materials and methods

2.1. Sample preparation

The chemicals and reagents used in this study were from the Sigma-Aldrich company. Zinc chloride ($ZnCl_2$), thiourea ($CS(NH_2)_2$), and aluminum sulfate $Al_2(SO_4)_3$ was employed as sources of zinc, sulfur, and aluminum, respectively.

The $ZnCl_2$ and CS (NH_2)$_2$ sample was immersed in methanol and added of the aluminum sulfate with different concentration. Next, the samples of Al 0, ZnS:Al 0.02, ZnS:Al 0.04, and ZnS:Al 0.06 films were prepared using pure (99.99%) elemental zinc and sulfur granules in predetermined mass ratios. The element of zinc and sulfur granules were weighed and placed in a clean silica glass tube.

Four different samples with aluminum in the proportion 0.00, 0.02, 0.04, and 0.06 were weighed and dopeted to the ZnS samples. The solutions obtained were thoroughly stirred to achieve homogeneity. After this, the homogenous sample was prepared into pellet of 2.0 mm thickness and 12.0 mm diameter with a hydraulic press of 5ton force for 35 min. The pellets were then sintered at 1200°C.

The soda-lime glass slides substrates were washed in succession with acetone, alcohol, and distilled water. The substrates moisture were removed using methanol. Further, the substrates were put in a container filled with a cleaning acidic surfactant solution. Following this, the substrates were immersed in an ultrasound bath for 10 minutes before the deposition.

2.2. Deposition of AZS thin films

The vacuum chamber of a vacuum coater was cleaned. The substrate wase mounted on the holder, and the ZnS and AZS samples were positioned on the boat. Nd: YAG laser (or Nd: $Y_3Al_5O_{12}$) in TEM00 mode used to facilitate the PLD method [26]. The laser source was operated in the wavelength of (λ = 532 nm) and 1064 nm, with a pulse number of 500. The laser repetition rate and pulse duration were 6Hz and 10 ns, respectively. Each sample was rotated as the laser rastered across the area of 0.5 cm^2 at an incident angle of 45° with a spot size of 3 mm^2. The fixed distance between the laser source and the target was 120 mm.

The films were grown under the laser fluence and energy of ~2 J/cm^2 and 100 mJ/pulse, respectively. The substrate–target distance was held constant at ~20 mm. Several tests were performed to create optimum conditions for the samples and the substrates. The pressure vacuum of the deposition chamber was 10^{-3} Torr.

2.3. Characterization of AZS films

XRD was performed to analyze the structure of the films, using a Cu-Kα radiation source with a wavelength (λ) of 0.1542 nm at 40 kV and 40 mA. A scanning rate of 0.026° per minute (2θ = 20–80°) was used.

3. Results and discussion

3.1. XRD results

The synthesized ZnS and Al-doped ZnS films of the XRD patterns are shown in Figure 1. The XRD patterns were recorded in the range 2θ = 20–80°, indexed as intense broadened peaks (111) and (200). The XRD images of the ZnS:Al 0, ZnS:Al 0.02, ZnS:Al 0.04, and ZnS:Al 0.06

films exhibited weak and broad peaks. Nonetheless, no other peak related to Al was seen in the patterns other than ZnS. This result indicates that the incorporation of Al into the films does not appear to alter any of the crystalline phase of ZnS. As shown, four diffraction peaks were observed at 28.29° and 30.76°, which corresponds to the (111) and (200) phases, respectively. A significant shift in the line-width of the ZnS film peak was observed when the Al doping level increased. This result shows that aluminum atoms in the ZnS lattice constant increases the crystal quality. This is consistent with previous studies' findings [27, 28].

The XRD images show that almost all the peaks concur with the ZnS wurtzite structure (JCPDS 36-1450) for the peaks (111) and (200) with $2\theta = 28.29°$ and 30.76°, respectively. The little peak at 39.25° concurs well with the (012) ZnS plane of zinc-blende structure (JCPDS 65-0309). The results show good agreement with the published data in the literature[29].

Figure 2 presents the XRD images of the crystal plane (111) and (200) diffraction peaks. The broad peaks came out as expected; the synthesized layers were nanocrystalline. All the XRD images of the AZS films exhibited peaks related to (111) and (200) orientations, which corresponds to the zinc-blende structure of ZnS [30]; the (111) plane was the dominant orientation.

The XRD spectra did not show any peaks related to secondary phases. Remarkably, as the Al concentration increased, the (111) peak became stronger. Although there was no significant alteration in the diffraction angles, there was a noticeable increment in the intensity, especially for high doping percentages of 4% and 6% Al.
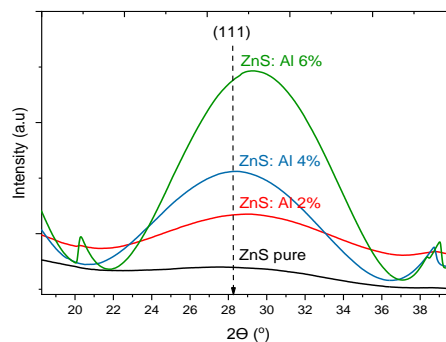

Figure 1. The XRD images of ZnS and AZS films.

However, the samples' peak positions shifted depending on the aluminum concentration. Figure 2 shows that, the peak shifts and widening in FWHM of (111), (200), and (012) reflection planes in Al-doped ZnS are indications of non-uniform strain during growth caused by embedding of the smaller ionic radii of Al^{3+} into the lattices ZnS NPs.

The Al^{3+} ion radius of 0.054 nm is smaller than that the Zn^{2+} ion radius of 0.074 nm, which forms strain in the films.
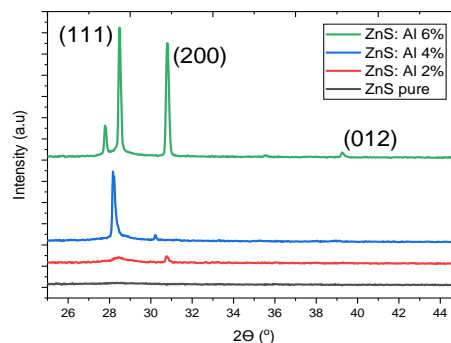

Figure 2. Images of ZnS and AZS films prepared by PLD
a) ZnS:Al 0.00, b) ZnS:Al 0.02, c) ZnS:Al 0.04, and d) ZnS:Al 0.06.

3.2. XRD Structural Parameters

The d-spacing d_{hkl} values were utilized to calculate the lattice constant [31] of the samples, which indicated mostly a cubic structure.

$$\frac{1}{d_{hkl}^2} = \frac{h^2+k^2+l^2}{a^2} \tag{1}$$

Here, *a* is lattice constant, d_{hkl} is the d-spacing related to Miller indices, *h*, *k*, and *l*. The d-spacing is for cubic unit cell structure at a = b = c.

The d-spacing reduces with increasing aluminum percentage. Table 1 presents the observed d-spacing data from XRD. The recorded d-spacing of 0.315, 0.312, 0.316, and 0.313 nm are in accordance with the reflection from crystal plane of the cubic structure, as shown in Table 1. The experimental d-spacing data matches are consistent with published values.

The reductions in the d-spacing of the ZnS films ranged from 0.315-0.313 nm nm in total, when aluminum increased , except in the case of 0.316 nm.

Table 1. The XRD images of ZnS and AZS films.

Sample	2θ (º)	d-spacing (nm)	FWHM β_{hkl} (º)
ZnS:Al 0.00	28.29	0.315	0.81
ZnS:Al 0.02	28.52	0.312	0.25
ZnS:Al 0.04	28.81	0.316	0.15
ZnS:Al 0.06	28.48	0.313	0.12

According to Table 1, FWHM value decreases as the Al concentration increases, which implies that the thin films become more crystalline directly depending upon the Al concentration. Debye Sherrer's formula was applied to calculate the particle grain size (D) based on the XRD pattern [32]:

$$D = \frac{n\lambda}{\beta_{hkl}cos\theta} \tag{2}$$

Here, D represents the crystallite grain size for the (hkl) plane; n is a constant; λ is the x-ray wavelength [Cu Kα (0.1542 nm)]; β_{hkl} is the Half Maximum of the Full-Width (FWHM) (in radians) of the most pronounced at the XRD peaks, and θ is the angle diffraction for the (hkl) plane. With increasing FWHM, the crystallite grain size decreased and vice versa [32].

Thus, a reduced FWHM and an increased grain size indicate better crystal quality. The summary of the parameters was devised from the XRD data of ZnS and AZS samples, that is, *D*, *δ*, and *ε*, are provided in Table 2.

Table 2. The crystal- size density and lattice strain of the ZnS and AZS films.

Sample	D (nm)	δ (mg.cm^{-3})	ε
ZnS:Al 0.00	0.80	1.54	0.0031
ZnS:Al 0.02	322.16	0.00000963	0.00095
ZnS:Al 0.04	537.35	0.00000346	0.00057
ZnS:Al 0.06	671.24	0.00000221	0.00046

When Al concentration increased, the crystal grain-size of the ZnS films increased from 0.80 nm to 671.24 nm. When the aluminum content inreases , the ZnS film density reduced from

1.54 mg.cm⁻³ to 0.00000221 mg.cm⁻³. Equation (4) was employed to find the induced strain (ε) of the ZnS and AZS samples [33]:

$$\varepsilon = \frac{\beta_{hkl} cos\theta}{4} \tag{4}$$

When the aluminum content inreases, the strain of the samples gradually decreased. This change could be because of (i) small grain formation because of nucleation during dopant incorporation into the host material, or (ii) stress resulting in disturbed grain growth because the difference in ion radius between zinc and aluminum. This changes in strain may due to the nature of the sample..

The dislocation density (δ) of the deposited films can be calculated using the following equation [33]:

$$\delta = \frac{1}{D^2} \tag{5}$$

Here, D is the crystal grain size. The value of the dislocation density of the film decreased with rising aluminum concentration. The dislocation density and strain are inversely proportional to each other when the films doped with the aluminum content as presented in Table 1.). Figure 3 presents a plot of the grain sizes and strain against aluminum concentrations. The films crystal grain size increased as the Al concentration increased. The results found in this study were consistent with the accepted findings [34].
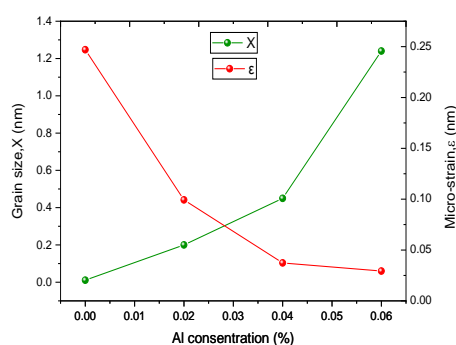

Figure 3. The plot of grain sizes and strain against Al concentration.

4. Conclusion

This study employed the PLD method to study undoped and Al-doped ZnS NPs of varying dopant concentrations. The XRD spectra of the samples revealed that the films grow in the cubic phase; specifically, they prefer too grow along the (111) direction. The d-spacing, crystallite grain size, strain, and dislocation density varied. The strain and the dislocation density of the film were inversely proportional with the crystallite size. Peak shifts and widening in FWHM of (111), (200), and (012) reflection planes in Al-doped ZnS were indications of non-uniform strain during growth, caused by embedding of the smaller ionic radii of Al³⁺ into the lattices of the ZnS films. This study shows encouraging results with respect to the optimizing the deposition parameters for possible optoelectronic applications of materials prepared using the PLD method.

References

[1] A. Jrad, T. B. Nasr, N. Turki-Kamoun, Mater Sci: Mater Electron 26, 8854 (2015).

[2] S. Ummartyotin, Y. Infahsaeng, A Renewable and Sustainable-Energy Reviews, 55, (17) (2016).

[3] A. Ganguly, S. S. Nath, V. M. Srivastava, Chalcogenide Letters, 17, (10), 487 (2020).

[4] S. Sharma, I. Singh, N. Chitkara, A. Kapoor, Materials Research Express 4 (7), 075046 (2017).

[5] K. Priya, V. K. Ashith, Gowrish K. Rao, Ganesh Sanjeev, Ceram. Int. 43, 10487 (2017).

[6] A. Phuruangrat, K. Karthik, B. Kuntalue, P. dumrongrojthanath, S. Thongtem, T. Thongtem, Chalcogenide Letters, 16, (8), 387 (2019).

[7] G. M. Jigi, T. Abza, A. Girma, Journal of Applied Bio-technology and Bio-engineering 8 (2), 55 (2021).

[8] G. Arandhara, P. K. Saikia, J. Bora, J. Bas. Appl. Eng. Res. 2 (20), 1761 (2015).

[9] M. N. Eman, Int. J. Innov. Res. Sci. Eng. Technol. 3, 8114 (2014).

[10] H. Benamra, H. Saidi, A. Attaf, M. S. Aida, A. Derbali, N. Attaf, Surfaces and Interfaces 21, 100645 (2020).

[11] A. I. Inamdar, Sangeun Cho, Yongcheol Jo, Kim Jongmin, Jaeseok Han, Materials Letters 163, 126 (2016).

[12] G. F. Aslan, A. Tumbul, Journal of Sol-Gel Sci. and Tech 75, 45 (2015).

[13] T. Hurma, Materials Science-Poland 37(4), 599 (2019).

[14] K. Nagamani, P. Prathap, Lingappa, R. W. Miles, K. T. R. Reddy, Phys. Procedia 25, 137 (2012).

[15] B. Long, S. Cheng, H. Zhou, J. Liao, H. Zhang, H. Jia, H. Li, ECS Solid State Lett. 3 (11), 140 (2014).

[16] A. Jrad, W. Naffouti, T. B. Nasr, N. Turki Kamoun, J. Lumin. 173, 135 (2016).

[17] F. Ozutok, K. Erturk, V. Bilgin, Acta Phys. Pol. A 121, 221 (2012).

[18] L. S. Donald, Thin-Film Deposition: Principles and Practice, McGraw-Hill, New York (1995).

[19] M. Sathishkumar, M. Saroja, M. Venkatachalam, Optik 182, 774 (2019).

[20] M. S. Bashar, R. Matin, M. Sultana, A. Siddika, M. Rahaman, M.A. Gafur. F. Ahmed, J. Theor. Appl. Phys. 14, 53 (2020).

[21] C. Sabitha, K. D. A. Kumar, S. Valanarasu, A. Saranya and H. Joe, Journal of Materials Science: Materials in Electronics, 29, 4612–4623 (2018).

[22] K. Priya, V. K. Ashith, K. R. Gowrish, Ganesh Sanjeev, Ceram. Int. 43, 10487 (2017).

[23] K. Nagamani, P. Prathap, Y. Lingappa, R. W. Miles, K. T. R. Reddy, Phys. Procedia 25, 137 (2012).

[24] K. R. Murali, S. Vasantha, K. Rajamma, properties of pulse plated ZnS films, Materials Letter 62, 1823 (2008).

[25] P. F. Luo, G. S. Jiang, C. F. Zhua, Chin. J. Chem. Phys, 22 (1), 97 (2009).

[26] M. H. Eisa, Materials Science in Semiconductor Processing 110, 104966 (2020).

[27] G. Nabiyouni, R. Sahraei, M. Toghiany, M. H. Majles Ara, K. Hedayati, Rev. Adv. Mater. Sci. 27, 52 (2011).

[28] V. H. Choudapura, S. B. Kapatkara, A. B. Rajub, Acta Chem. Iasi 27(2), 287 (2019).

[29] X. H. Zeng, S. Yan, J. Y. Cui . H. F. Liu, J. Dong, W. W. Xia, M. Zhou, H. T. Chen, J Nanopart Res 17, 188 (2015).

[30] A. H. Eid, S. M. Salim, M. B. Sedik, H. Omar, T. Dahy, H. M. Abou-Elkhair, J. Appl. Sci. Res. 6 (6), 777 (2010).

[31] F. Haque, K. S. Rahman, M. A. Islam, M. J. Rashid, M. Akhtaruzzaman, M. M. Alam, Z. A. Alothman, K. Soplan, N. Amin, Chalcogenide Letters 11(40), 189 (2014).

[32] C. Zörer, O. Baytar, Ö. Şahin, S. Horoz, M. S. Izgi, Digest Journal of Nanomaterials

and   Biostructures 15 (3), 629 (2020).

[33] M. M. Ali, Basrah J. Sci. A 33 (1), 156 (2015).

[34] Y. Infahsaeng, S. Ummartyotin, Results in Physics 7, 1245 (2017).